MECSOL 2019 - Proceedings of the 7th International Symposium on Solid Mechanics
V. Tita, A. Ferreira, M.L. Ribeiro, A. Vieira and A.T. Beck (Editors), ABCM, Sao Carlos, SP, Brazil, April 15th to 17th, 2019

Isogeometric Shell Analysis based on Kirchhoff-Love theory

Jorge G. Zúñiga[1], Roberto D. Machado[1], Marcos Arndt[1]

[1] Graduation Program in Numerical Methods in Engineering (PPGMNE), Centro Politécnico, Federal University of Paraná (UFPR), Mailbox 19.011, CEP 81.531-980, Curitiba – Paraná.

Abstract. In this work, the isogeometric concept is applied to the analysis of shell structures. A rotation-free element is developed, using the Kirchhoff-Love theory and NURBS as basic functions. An analysis based on NURBS provides advantages especially for shells, since the structural behavior of a shell is mainly determined by its geometry and therefore a good description of the geometry is essential. In addition, due to the exact description of the geometry with NURBS, the curvatures can be evaluated directly on the surface without rotational degrees of freedom. Different examples show the good performance and precision of the method, for problems with geometric linearity.
Keywords: Isogeometric Analysis, NURBS, B-Splines, Kirchhoff-Love.

INTRODUCTION

A shell is a thin-walled structure with arbitrary curvature in the three-dimensional space. A shell transmits the load through its shape and therefore, is very efficient to save material and weight, due its curvature. The transverse loads can be transmitted by traction and compression, while bending moments are minimized. This behavior allows a very efficient use of the material. The isogeometric analysis (IGA) is a new method of computational analysis with the objective of combining the design and the analysis in a single model using a unified geometric representation. Since there is not losing information when transferring the design model to the analysis model, is a great advantage on the traditional finite element method (FEM), where the analysis model is only an approximation of the design model. NURBS (Non-Uniform Rational B-Spline) is the most widely used technology in today's CAD (Computer Aided Design) modeling tools and is therefore adopted as the basic functions for analysis.

NURBS AND ISOGEOMETRIC ANALYSIS

NURBS are a generalization of B-Splines and most of the features of NURBS also apply to B-Splines, so first a short introduction to B-Splines is given.

B-Splines

A B-Spline is a non-interpolating, piecewise polynomial curve. It is defined by a set of control points $\mathbf{P}_i$, the polynomial degree p and a so called knot vector $\Xi = [\xi_1, \xi_2, ..., \xi_{n+p+1}]$. The knot vector is a set of parametric coordinates ξ_i in non-descending order which divide the B-Spline into sections. If all knots are equally spaced, the knot vector is called uniform. A B-Spline basis function is C^∞ continuous inside a knot span, i.e. between two distinct knots, and C^{p-1} continuous at a single knot. A knot value can appear more than one time and is then called a multiple knot. At a knot of multiplicity k the continuity is C^{p-k}. If the first and the last knot have the multiplicity $p+1$, the knot vector is called open (Piegl and Tiller, 1997). In a B-Spline with an open knot vector the first and the last control point are interpolated and the curve is tangential to the control polygon at the start and the end of the curve. Open knot vectors are standard in CAD applications and are assumed for the remainder of this text.

Basis functions

B-Spline basis functions are computed by the Cox–deBoor recursion formula (Piegl and Tiller, 1997). It starts for $p = 0$ with:

$$N_{i,p}(\xi) = \begin{cases} 1 & \text{se } \xi_i \leq \xi < \xi_{i+1}, \\ 0 & \text{otherwise.} \end{cases} \tag{1}$$

For $p \geq 1$ it is

$$N_{i,p}(\xi) = \frac{\xi - \xi_i}{\xi_{i+p} - \xi_i} N_{i,p-1}(\xi) + \frac{\xi_{i+p+1} - \xi}{\xi_{i+p+1} - \xi_{i+1}} N_{i+1,p-1}(\xi). \tag{2}$$

From this formulation some important properties of B-Spline basis functions can be deduced:

- Local support, i.e. a basis function $N_{i,p}(\xi)$ is non-zero only in the interval $[\xi_i, \xi_{i+p+1}]$.
- Partition of unity, i.e. $\sum_{i=1}^{n} N_{i,p}(\xi) = 1$.
- Non-negativity, i.e. $N_{i,p}(\xi) \geqslant 0$.
- Linear independence, i.e. $\sum_{i=1}^{n} \alpha_i N_{i,p}(\xi) = 0 \Longleftrightarrow \alpha_j = 0, j = 1, 2, ..., n$.

Figure (1.a) shows an example of quadratic B-Spline basis functions with an open knot vector.

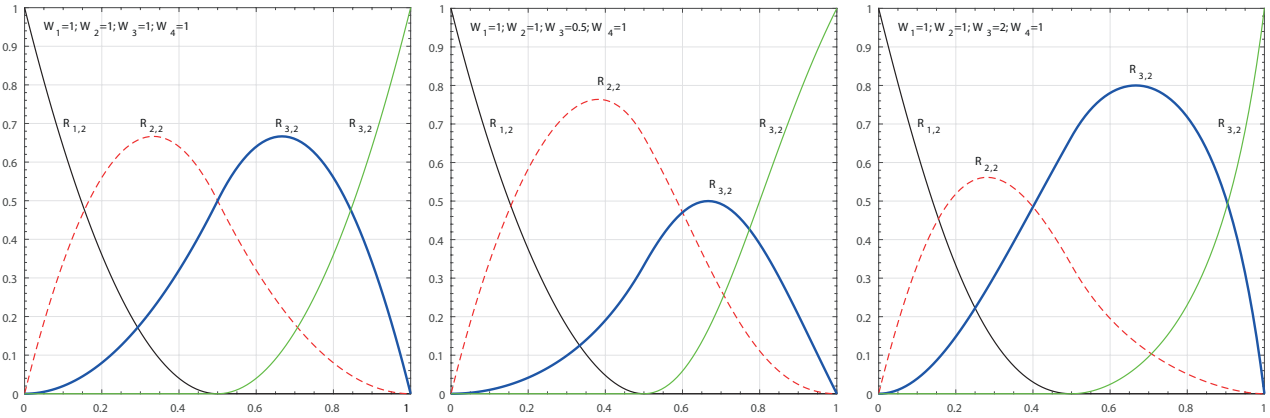

(a) *B-Spline Basic functions ($p = 2$).*

(b) *NURBS Basic functions ($p = 2$), with weight $W_3 = 0.5$.*

(c) *NURBS Basic functions ($p = 2$), with weight $W_3 = 2.0$.*

Figure 1 – *Quadratic B-Spline and NURBS base functions with open knot vector*
$\Xi = [\xi_1, \xi_2, \xi_3, \xi_4, \xi_5, \xi_6, \xi_7] = [0, 0, 0, 0.5, 1, 1, 1]$.

B-Spline curves

A B-Spline curve of degree p is computed by the linear combination of control points and the respective basis functions:

$$\mathbf{C}(\xi) = \sum_{i=1}^{n} N_{i,p}(\xi) \mathbf{P}_i. \tag{3}$$

Figure (2) shows an example of a quadratic B-Spline curve (blue curve) with an open knot vector. Due to the open knot vector the first and last control point (P1 and P4) are interpolable and it can be seen that the curve is tangential to the control polygon at its beginning and end.

B-Spline surfaces

A B-Spline surface is computed by the tensor product of BSpline basis functions in two parametric dimensions ξ and η. It is defined by a net of $n \times m$ control points, two knot vectors Ξ and H, two polynomial degrees p and q (which do not need to be equal), and correspondingly the basis functions $N_{i,p}(\xi)$ and $M_{j,q}(\eta)$. It is described as:

$$\mathbf{S}(\xi, \eta) = \sum_{i=1}^{n} \sum_{j=1}^{m} N_{i,p}(\xi) M_{j,q}(\eta) \mathbf{P}_{i,j}. \tag{4}$$

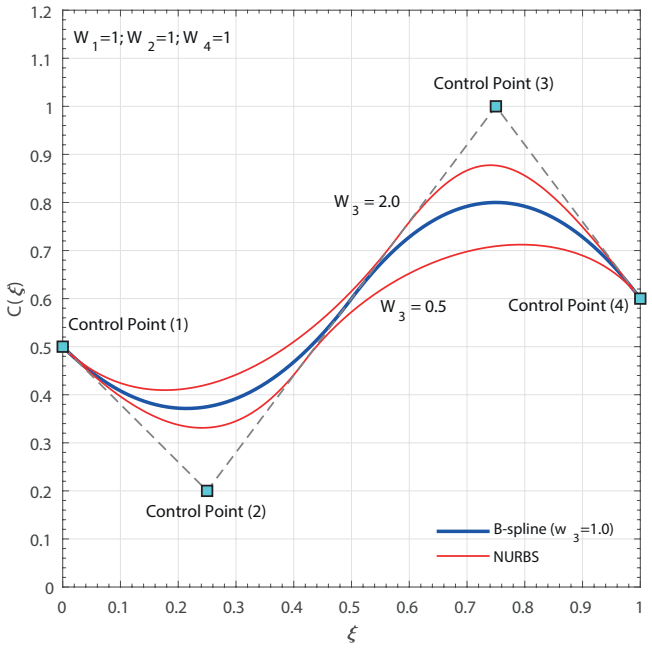

Figure 2 – ***Curves B-Spline (blue color) and NURBS (red color) with open knot Vector*** $\Xi = [0,0,0,0.5,1,1,1]$***. The dashed line represents the control polygon and the small squares represent the control points. The first and last control point are interpolated and the curve is tangent to the control polygon at its beginning and end.***

Figure (3) shows an example of a quadratic B-Spline surface and its control net. Due to the open knot vectors the control points at the vertices of the surface are interpolated. The black lines on the surface mark the knots which divide the surface into elements.

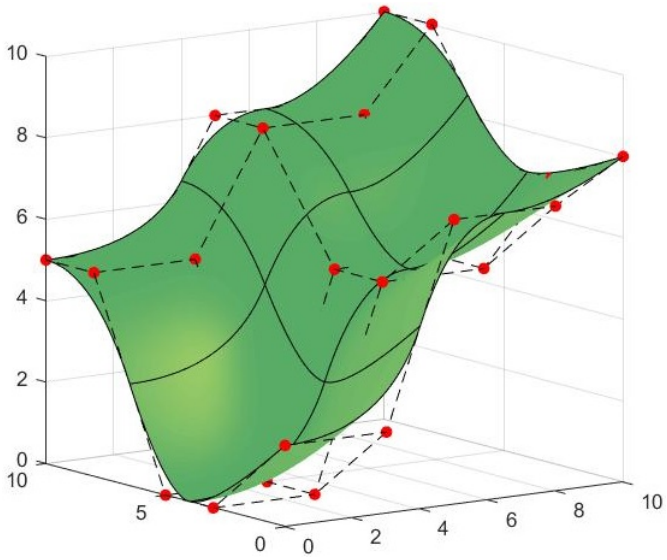

Figure 3 – ***Quadratic B-Spline surface with open knot vectors*** $\Xi = H = [0,0,0,1/3,2/3,1,1,1]$***. The control polygon is shown in black color with dashed line and the control points are the circles of red color. Due to the open knot vectors the control points at the vertices of the surface are interpolable. The black lines on the surface mark the nodes which they divide to the surface into elements (subregions).***

NURBS

NURBS are nonuniform rational B-Splines. For NURBS each control point has additionally to its coordinates an individual weight w_i. Such a point $\mathbf{P}_i(x_i, y_i, z_i, w_i)$ can be represented with homogeneous coordinates $\mathbf{P}_i^w(w_i x_i, w_i y_i, w_i z_i, w_i)$ in a projective $\mathbb{R}^4$ space. A NURBS curve is the projection of a B-Spline in $\mathbb{R}^4$ with homogeneous control points onto $\mathbb{R}^3$ (Cottrell et al., 2009)(Piegl and Tiller, 1997), In Fig.(1.b) and (1.c) one can see the effect of the weights on the basic functions:

$$\mathbf{C}(\xi) = \frac{\sum_{i=1}^{n} N_{i,p}(\xi) w_i}{\sum_{\hat{i}=1}^{n} N_{\hat{i},p}(\xi) w_{\hat{i}}} \mathbf{P}_i. \tag{5}$$

In a compact way Eq.(5) is,

$$\mathbf{C}(\xi) = \sum_{i=1}^{n} R_i^p(\xi) \mathbf{P}_i. \tag{6}$$

In Fig. (1.b), (1.c) and (2), it can be seen that a higher order weight value $(W_3 = 2.0)$ shifts the curve toward the third control point and a value of lower order weight $(W_3 = 0.5)$ moves the curve from the control point. This additional flexibility makes NURBS so attractive to describe geometries.
A NURBS surface is defined as:

$$\mathbf{S}(\xi, \eta) = \frac{\sum_{i=1}^{n} \sum_{j=1}^{m} N_{i,p}(\xi) M_{j,q}(\eta) w_{i,j}}{\sum_{\hat{i}=1}^{n} \sum_{\hat{j}=1}^{m} N_{\hat{i},p}(\xi) M_{\hat{j},q}(\eta) w_{\hat{i},\hat{j}}} \mathbf{P}_{i,j}. \tag{7}$$

In a compact way Eq. (7) is,

$$\mathbf{S}(\xi, \eta) = \sum_{i=1}^{n} \sum_{j=1}^{m} R_{i,j}^{p,q}(\xi, \eta) \mathbf{P}_{i,j}. \tag{8}$$

NURBS are able to exactly represent some important geometric entities, like e.g. conic sections (i.e. circles, cylinders, spheres, etc.). Moreover, a B-Spline is a special case of a NURBS where all weights are equal and is therefore automatically contained in all the subsequent derivations for NURBS-based elements.

Mesh refinement

There are two ways of mesh refinement analogous to standard FE, namely knot insertion and order elevation.

Knot insertion (h-refinement)

The knot spans can be divided into smaller ones by inserting new knots. This corresponds to h-refinement in classical FE analysis (Zienkiewicz et al., 2005). Inserting knots does neither change the geometry nor the parametrization.

Order elevation (p-refinement)

Analogous to p-refinement the polynomial degree of the basis functions can be increased. While increasing the order, existing knots have to be repeated so that the continuity between them remains unchanged. Similarly to knot insertion, order elevation does neither change the geometry nor the parametrization. For both knot insertion and order elevation new control points have to be computed. When applying them to NURBS the computation of the refined curve has to be done in the projective space with homogeneous coordinates. For a detailed description see (Piegl and Tiller, 1997).

K-refinement

Introduced in (Hughes et al., 2005), k-refinement is a combination of p- and h-refinement. This process is not commutative, p-refinement results in base functions with C^0 continuity at the boundaries of elements while refinement-k provides functions with C^{p-1} continuity.

NURBS as basis for FE analysis

Using NURBS as basis for the analysis is one possibility to merge design and analysis. Alternatives could be using subdivision surfaces or B-Splines. For our work we used the NURBS based isogeometric approach as proposed by Hughes (Hughes et al., 2005) (Cottrell et al., 2009) where the NURBS patch defines a subdomain and the elements are defined by the knot spans of this patch. This means that each basis function has support on a small number of elements (depending on the polynomial degree). The isoparametric concept is used, i.e. the geometry and the displacement are described by the same basis functions. The displacements of the control points are the degrees of freedom of the structure. Numerical integration is done by Gauss quadrature on element level (Hughes, 2012).

FORMULATION BY SUB-REGIONS

In the Kirchhoff–Love shell theory (Beer, 2015)(Kiendl et al., 2009) transverse shear deformationis neglected and the director, i.e. a vector normal to the middle surface, remains normal to the middle surface in the deformed configuration. Therefore, the description of the shell can be reduced to the description of its middle surface, generalize the geometry to include curvature and introduce 3 components for the unknown $\mathbf{u}$ (u_x, u_y, u_z). The displacement field is now approximated by:

$$\mathbf{u} = \sum_{n=1}^{I} R_n(\xi,\eta)\mathbf{u}_n; \qquad \mathbf{u}_n = \begin{bmatrix} u_{xn} \\ u_{yn} \\ u_{zn} \end{bmatrix}. \tag{9}$$

The membrane strain vector are defined as,

$$\boldsymbol{\varepsilon}_m = \begin{bmatrix} \varepsilon_x \\ \varepsilon_y \\ \tau_{xy} \end{bmatrix} = \begin{bmatrix} \dfrac{\partial u_x}{\partial x} \\ \dfrac{\partial u_y}{\partial y} \\ \dfrac{\partial u_x}{\partial y} + \dfrac{\partial u_y}{\partial x} \end{bmatrix}; \quad \boldsymbol{B}_i^m = \begin{bmatrix} \dfrac{\partial R_i}{\partial x} & 0 \\ 0 & \dfrac{\partial R_i}{\partial y} \\ \dfrac{\partial R_i}{\partial y} & \dfrac{\partial R_i}{\partial x} \end{bmatrix}. \tag{10}$$

The bending strain vector are defined as,

$$\boldsymbol{\varepsilon}_b = \begin{bmatrix} \varepsilon_x \\ \varepsilon_y \\ \tau_{xy} \end{bmatrix} = \begin{bmatrix} z \cdot \dfrac{\partial^2 u_z}{\partial x} \\ z \cdot \dfrac{\partial^2 u_z}{\partial y} \\ 2 \cdot z \cdot \dfrac{\partial^2 u_z}{\partial x \partial y} \end{bmatrix}; \quad \boldsymbol{B}_i^b = \begin{bmatrix} \dfrac{\partial^2 R_i}{\partial \xi^2} \\ \dfrac{\partial^2 R_i}{\partial \eta^2} \\ 2 \cdot \dfrac{\partial^2 R_i}{\partial \xi \partial \eta} \end{bmatrix}. \tag{11}$$

The stress-strain relationship is deduced as,

$$\boldsymbol{\sigma} = \boldsymbol{D}(\boldsymbol{\varepsilon}_m - z \cdot \boldsymbol{\varepsilon}_b); \quad \boldsymbol{\varepsilon} = (\boldsymbol{\varepsilon}_m - z \cdot \boldsymbol{\varepsilon}_b). \tag{12}$$

Where a constitutive matrix $\boldsymbol{D}$ is composed of the following matrices:

$$\boldsymbol{D}_m = \frac{Et}{1-\nu^2} \begin{bmatrix} 1 & \nu & 0 \\ \nu & 1 & 0 \\ 0 & 0 & 0.5(1-2\nu) \end{bmatrix}; \boldsymbol{D}_b = \frac{Et^3}{12(1-\nu^2)} \begin{bmatrix} 1 & \nu & 0 \\ \nu & 1 & 0 \\ 0 & 0 & 0.5(1-2\nu) \end{bmatrix}. \tag{13}$$

We now separate the membrane and the bending terms and compute two $\boldsymbol{B}$ matrices, $\boldsymbol{B}^m$ for the membrane terms and $\boldsymbol{B}^b$ for the bending terms. The matrix associated with the membrane strains is given by:

$$\boldsymbol{B}_i^m = \begin{bmatrix} m_1^i \cdot v_{1x} & m_1^i \cdot v_{1y} & m_1^i \cdot v_{1z} \\ m_2^i \cdot v_{2x} & m_2^i \cdot v_{2y} & m_2^i \cdot v_{2z} \\ 0.5(m_1^i \cdot v_{2x} + m_2^i \cdot v_{1x}) & 0.5(m_1^i \cdot v_{2y} + m_2^i \cdot v_{1y}) & 0.5(m_1^i \cdot v_{2z} + m_2^i \cdot v_{1z}) \end{bmatrix}. \tag{14}$$

where,

$$m_1^i = \frac{\partial R_i}{\partial \xi}; \quad m_2^i = \frac{\partial R_i}{\partial \eta}. \tag{15}$$

The matrix for the bending terms is given by:

$$\boldsymbol{B}_i^b = \begin{bmatrix} b_{11}^i \cdot n_x & b_{11}^i \cdot n_y & b_{11}^i \cdot n_z \\ b_{22}^i \cdot n_x & b_{22}^i \cdot n_y & b_{22}^i \cdot n_z \\ b_{12}^i \cdot n_x & b_{12}^i \cdot n_y & b_{12}^i \cdot n_z \end{bmatrix}, \tag{16}$$

where,

$$\begin{aligned} b_{11}^i &= \frac{\partial^2 R_i}{\partial \xi^2} - E_{11}^1 \cdot \frac{\partial R_i}{\partial \xi} - E_{11}^2 \cdot \frac{\partial R_i}{\partial \eta}, \\ b_{22}^i &= \frac{\partial^2 R_i}{\partial \eta^2} - E_{22}^1 \cdot \frac{\partial R_i}{\partial \xi} - E_{22}^2 \cdot \frac{\partial R_i}{\partial \eta}, \\ b_{12}^i &= 2 \cdot \left(\frac{\partial^2 R_i}{\partial \xi \partial \eta} - E_{12}^1 \cdot \frac{\partial R_i}{\partial \xi} - E_{12}^2 \cdot \frac{\partial R_i}{\partial \eta} \right), \end{aligned} \tag{17}$$

and,

$$\begin{aligned} E_{11}^1 &= \frac{1}{J}\left[(v_2 \times N) \cdot \frac{\partial^2 x}{\partial \xi^2} \right]; \;\; E_{11}^2 = \frac{1}{J}\left[(N \times v_1) \cdot \frac{\partial^2 x}{\partial \xi^2} \right]; \\ E_{22}^1 &= \frac{1}{J}\left[(v_2 \times N) \cdot \frac{\partial^2 x}{\partial \eta^2} \right]; \;\; E_{22}^2 = \frac{1}{J}\left[(N \times v_1) \cdot \frac{\partial^2 x}{\partial \eta^2} \right]; \\ E_{12}^2 &= \frac{1}{J}\left[(v_2 \times N) \cdot \frac{\partial^2 x}{\partial \xi \partial \eta} \right]; \;\; E_{12}^2 = \frac{1}{J}\left[(N \times v_1) \cdot \frac{\partial^2 x}{\partial \xi \partial \eta} \right]; \end{aligned} \tag{18}$$

Using the principle of virtual works, we apply virtual displacements $\delta \boldsymbol{u}_i$ and calculate the internal virtual work,

$$\delta W_{int} = -\int_V \boldsymbol{\sigma}^T \delta \boldsymbol{\varepsilon} \cdot dV. \tag{19}$$

After replacing the Eq.(12) in Eq.(19) we get,

$$\delta W_{int} = -\int_V \left[\boldsymbol{D} \sum_{i=1}^{I} \boldsymbol{B}_i \cdot \mathbf{u}_i \right]^T \boldsymbol{B}_j \cdot \delta \mathbf{u}_j \cdot dV. \tag{20}$$

The stiffness matrix of each sub-region is given by:

$$\mathbf{k}_{i,j}^s = \int_{-1}^{+1} \int_{-1}^{+1} \left[(\boldsymbol{B}_i^m)^T \cdot \boldsymbol{D}_m \cdot \boldsymbol{B}_j^m + \left(\boldsymbol{B}_i^b \right)^T \cdot \boldsymbol{D}_b \cdot \boldsymbol{B}_j^b \right] \cdot J_\xi \cdot \det J \cdot d\xi \cdot d\eta, \tag{21}$$

Now the numerical integration for the stiffness matrix is given by:

$$\mathbf{k}_{i,j}^s = \sum_{k=1}^{K} \sum_{m=1}^{M} \sum_{n=1}^{N} \left[(\boldsymbol{B}_i^m(\xi_n, \eta_m))^T \cdot \boldsymbol{D}_m \cdot \boldsymbol{B}_j^m(\xi_n, \eta_m) + \left(\boldsymbol{B}_i^b(\xi_n, \eta_m) \right)^T \cdot \boldsymbol{D}_b \cdot \boldsymbol{B}_j^b(\xi_n, \eta_m) \right] \cdot J_\xi \cdot \det J(\xi_n, \eta_m) \cdot W_n \cdot W_m. \tag{22}$$

Where M and N are the number of Gauss points, K is the number of sub-regions, $\det J(\xi_n, \eta_m)$ is the Jacobian determinant, W_n and W_m are the Gaussian weights and J_ξ is the value that allows Gaussian points to be transformed from the Gaussian space to the parametric space.

TEST PROBLEM

In this section, a numerical example in linear elasticity and with double curvature, is presented with the purpose to serve as a verifcation example for IGA.

Pinched hemisphere

The problem consists of a hemisphere that is fixed at its top point and subjected to concentrated forces on the free boundary. The forces are applied in opposite direction along the global x and y axes as shown in Fig. (4). The reference for the converged solution is given in terms of radial displacement at the loaded points, $u = 0.0924\ m$ (Macneal and Harder, 1985). Only one quarter of the shell is modeled given the double symmetry. The symmetry conditions are applied by the penalty method in the isogeometric shell model.

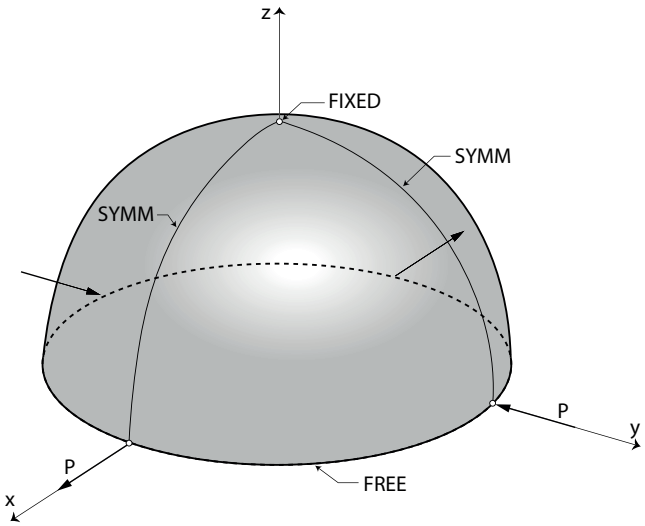

Figure 4 – ***the shell is fixed at its top point and subjected to opposite concentrated forces on the free boundary. Only one quarter of the shell is modeled due to symmetry.***

Remaining data for the problem setup is given in the Tab. (1) below:

Table 1 – Mechanical and geometric properties of the model.

Variable	Value	Unit
Young's modulus, E	$6.825 \cdot 10^7$	$[Pa]$
Thickness of shell, t	0.04	$[m]$
Angle, φ	2π	$[rad]$
Poisson's ratio, v	0.30	$[-]$
Radius, R	10	$[m]$
Point loads, P	± 2	$[N]$

The convergence to the reference value for the loaded point on the x-axis is shown in Fig. (5). As can be seen, higher polynomial degrees give both a better initial approximation and stronger convergence rate.

In order to have an overall idea of accuracy and stability, a comparison is made between the relative error in strain energy versus number of degrees of freedom. Six models are produced for the test problem. The polynomial degrees range from $p = 2$ to $p = 7$ and $q = 2$ to $q = 7$, where p and q are the degrees of the polynomials in the parametric direction ξ and η respectively.

For the quantitative comparison, we consider the strain energy of the solution:

$$E = \frac{1}{2}\|u\|^2, \tag{23}$$

$$\|\cdot\| = \sqrt{a(\cdot,\cdot)}, \tag{24}$$

where $a(\cdot,\cdot)$ pertains to the "energy" product of the mechanical equilibrium. For a discrete approximation, we then obtain:

$$E_h = \frac{1}{2}a(u_h,u_h) = \frac{1}{2}\boldsymbol{a}^T\boldsymbol{K}\boldsymbol{a}, \tag{25}$$

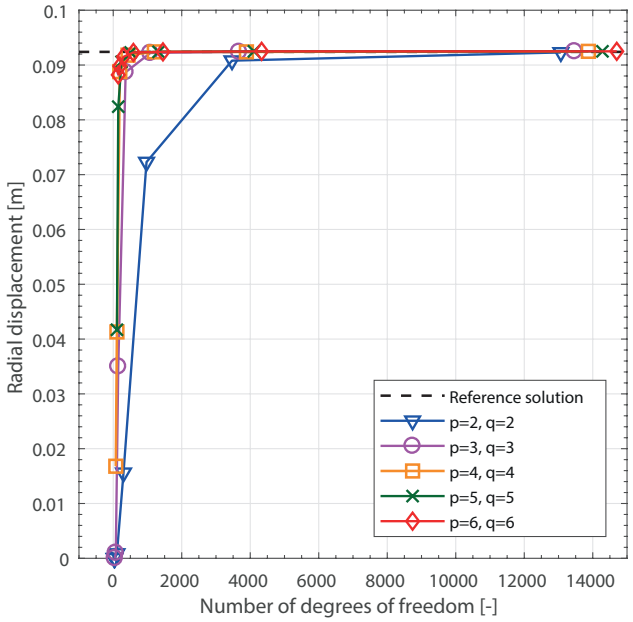

Figure 5 – ***Convergence of radial displacement at the loaded point on the global x-axis.***

With h denoting the approximate solution and ref the analytical reference solution, the relative error can be expressed as:

$$e_{ref} = \left| \frac{E_{ref} - E_h}{E_{ref}} \right|. \tag{26}$$

The results, seen in Fig. (6), show that the convergence is smooth, the most accurate analysis setup with the highest convergence rate is given by IGA with $p = q = 7$. In general it is seen that the IGA solutions with $p, q \geqslant 3$ have excellent convergence rate.

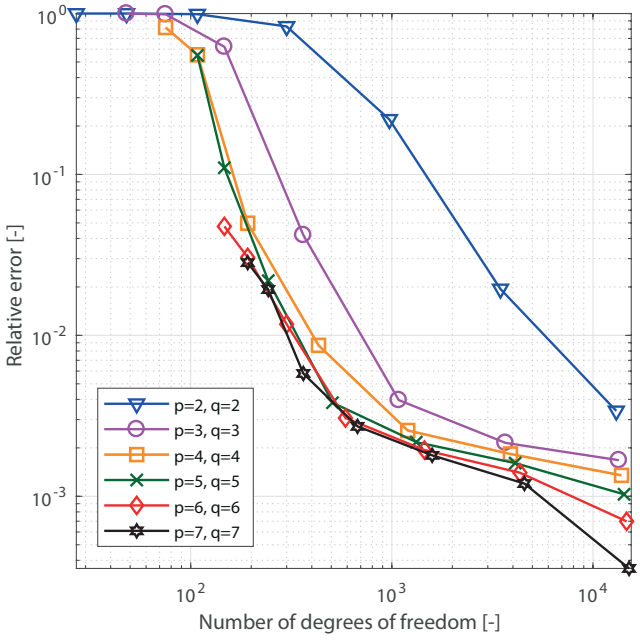

Figure 6 – ***Convergence of the relative error in strain energy versus number of degrees of freedom.***

CONCLUSIONS

- From the results obtained, we can conclude that IGA applied to shell structures provides excellent results both in terms of accuracy and convergence rate.
- A key factor is the ability to utilize higher continuity over element boundaries compared to classic finite element method.

REFERENCES

Beer, G., 2015, "Advanced numerical simulation methods: from CAD data directly to simulation results", CRC press.

Cottrell, J.A., Hughes, T.J. and Bazilevs, Y., 2009, "Isogeometric analysis:Toward integration of CAD and FEA", John Wiley & Sons.

Hughes, T.J., 2012, "The finite element method: linear static and dynamic finite element analysis", Courier Corporation.

Hughes, T.J., Cottrell, J.A. and Bazilevs, Y., 2005, "Isogeometric analysis: CAD, finite elements, NURBS, exact geometry and mesh refinement", Computer methods in applied mechanics and engineering 194, Nr.39-41, S.4135–4195.

Kiendl, J., Bletzinger, K., Linhard, J. and Wuchner, R., 2009, "Isogeometric shell analysis with Kirchhoff– Love elements" , Computer Methods in Applied Mechanics and Engineering 198, Nr.49-52, S.3902–3914.

Macneal, R.H. and Harder R.L., 1985, "A proposed standart set of problems to test finite element accuracy", Elsevier Science Publishers, North-Holland.

Piegl, L. and Tiller, W., 1997, "The NURBS book 2nd Ed", Springer-Verlag, New York.

Zienkiewicz, O.C., Taylor, R.L., Zhu, J.Z., 2005, "The Finite Element Method: Its Basis and Fundamentals", Butterworth-Heinemann.

RESPONSIBILITY NOTICE

The authors are the only responsible for the printed material included in this paper.